RSC Advances

PAPER

View Article Online
View Journal | View Issue

Cite this: *RSC Adv.*, 2025, **15**, 45453

Improving the conversion of petroleum coke to solid acid catalysts – effectiveness of hydrogen peroxide and impact of silica contamination

Natalia Mariano Cabral and Josephine M. Hill *

Petroleum coke (petcoke) samples containing silica sand (SiO_2) in the concentrations of ~50 and 7 wt% were functionalized with nitric acid and hydrogen peroxide to produce carbon-based solid acid catalysts by converting the inherent sulfur species in petcoke to sulfonic acid sites ($-SO_3H$). The effect of SiO_2 content and functionalization agent on the physical, surface, and acidic properties of the prepared materials were evaluated, and their catalytic activities were assessed in the esterification reaction of octanoic acid and methanol at 60 °C, yielding 17–54% of ester after 6 h. The functionalization with H_2O_2 is more environmentally friendly than with HNO_3 and produces more active catalysts (ester yields of 54% and 45%, respectively). The activities of the prepared materials were more dependent on having fewer oxygen-containing carbon groups (related to total acidity) on the surface than on a higher concentration of sulfonic acid sites. Thus, the improved activity of the catalyst prepared with H_2O_2 was due to a lower total acidity (~1 mmol g^{-1}) than the catalyst prepared with HNO_3 (~5 mmol g^{-1}). The stabilities of petcoke-derived catalysts were poor, and regeneration was not possible, which is a common problem for carbon-based solid acid catalysts. The petcoke with a higher content of SiO_2 resulted in better esterification performance. The silica sand promoted the reduction of particle size during the ball-milling process, leading to reduced diffusion limitations and the generation of silanol groups that are hydrogen-bond donors, helping in the esterification reaction.

Received 12th August 2025
Accepted 10th November 2025

DOI: 10.1039/d5ra05900c

rsc.li/rsc-advances

Introduction

Petroleum coke (petcoke) is a solid by-product from the refining of crude oil and upgrading of bitumen. This carbon-rich material (>80 wt%) also contains hydrogen, nitrogen, oxygen, sulfur (1–8 wt%), and several trace elements,[1] and is stockpiled at a rate of ~6 million tonnes per year globally.[2] The sulfur content limits the direct use of petcoke, and as the piles of petcoke are open to the atmosphere, the release of pollutants – volatile organic and aromatic compounds – to the air and groundwater is a problem.[3] Thus, researchers have been exploring ways to valorize this feedstock, including as an adsorbent for heavy metals sequestration,[4] a precursor for the preparation of carbon-based nanomaterials,[5] supercapacitors,[6] a support for photocatalysts,[7] a co-gasification feed with biomass,[8] adducts in construction materials,[9] and a solid acid catalyst.[10–13] While various reactants can be used to convert the petcoke to these products, many of these reactants are not environmentally friendly.

The sulfur species in petcoke were reported to be mainly organic compounds, accounting for more than 90 wt% of the total sulfur, and the remaining were inorganic species (sulfates). The organic fraction contains dominantly thiophene, benzothiophene, and dibenzothiophene molecules (60–80 wt%), 10–30 wt% of sulfoxide, and a minor fraction (<10 wt%) of sulfides/disulfides.[12,14–16] These thiophenes have high thermal stability, making their removal hard to accomplish. However, they can be converted through an oxidation process. Strong acids are often used as oxidizers; nitric acid, for example, is effective at converting the inherent organic sulfur into sulfonic acid sites ($-SO_3H$)[12,13] but releases NO_x gases and promotes SO_2 formation during its decomposition in the petcoke functionalization process.[13,17] After oxidation with nitric acid, the sulfur content in petcoke was reported to decrease around 20–40 wt% due to SO_2 formation, and the sulfur species were reported to be exclusively organic, in which 10–30 wt% were oxidized sulfur ($-SO_3H$), and the remaining was thiophenic compounds.[12,13]

Solid-acid catalysts from petcoke were also prepared in a two-step process involving chemical activation with KOH and sulfonation with H_2SO_4.[18,19] Another study applied chemical activation with KOH and impregnation with ammonium heptamolybdate to enhance the mesoporosity, then used functionalization with HNO_3 to convert petcoke into a mesoporous solid acid catalyst.[11] These activation processes resulted in the removal of sulfur from petcoke.[20] For the conversion of other

Department of Chemical & Petroleum Engineering, Schulich School of Engineering, University of Calgary, 2500 University Dr NW, Calgary, AB, T2N 1N4, Canada. E-mail: jhill@ucalgary.ca; Fax: +1 403 284 4852; Tel: +1 403 284 4519

carbon materials, such as agricultural waste, researchers have used mainly concentrated acids (*e.g.*, H_2SO_4, HNO_3, and H_3PO_4) *via* a sulfonation process to introduce acidity to the surface of the carbon material. Before the sulfonation, however, most waste carbon feedstocks were modified with carbonization, pyrolysis or activation.[21–26] Based on sulfur conversion pathways predicted *via* density functional theory (DFT) calculations, $^{\bullet}OH$ is formed and could contribute to the oxidation of sulfur in petcoke.[13] Therefore, hydrogen peroxide, which decomposes to water, may be effective because it produces these radicals but is less active for carbon oxidation compared to HNO_3 [27,28] and so will result in fewer undesirable surface groups (*i.e.*, carbonyl, carboxyl, and hydroxyl).

Aside from the components within the petcoke, other contaminants may be introduced from the extraction, processing, and storage steps.[29–35] Petcoke is one of many waste materials that contains silica. Agricultural waste, such as rice husk, sugar cane bagasse, wheat husk, and corn straw, may contain up to 50–86 wt% silica/silicon in the ash.[36–39] Similar to petcoke, the harvesting, handling, and storage processes of these agricultural wastes can incorporate soil, resulting in a SiO_2 concentration of 2–25 wt% in these feedstocks.[38,39] Silica is generally an inert material for many reactions but may damage the process equipment because of its hardness. This material is also detrimental to the valorization of other waste feedstocks, affecting the feasibility of the pyrolysis of waste tires to value-added products,[40] and inhibiting the biogas production from sewage sludge.[41] Separation of the silica before processing the material, however, adds complexity and cost to the overall process, possibly negating the benefits of using a waste feedstock.

In this study, petcoke-derived solid acid catalysts were prepared using hydrogen peroxide to access the sulfur species and convert them to sulfonic acid sites and were characterized with various techniques. Two batches of petcoke with different silica contents were used to evaluate the effect of SiO_2 on the functionalization process and subsequent activity of the produced catalysts. The reaction of octanoic acid and methanol to produce an ester was used to evaluate the catalysts. Esterification reactions such as this one are part of the route to convert biomass, a renewable resource, into biodiesel.

Experimental

Materials and methods

Materials. The delayed petcoke (PC) from the oil sands industry used in this work was supplied by Suncor Energy Inc., Alberta, Canada. The two batches contained different levels of silica. The batch with the higher ash content (~50 wt%) is referred to as PCSi, while the batch with the lower ash content (~7 wt%) is referred to as PC. Before any experiments, samples from both batches were ground and sieved into particles in the range of 20–100 μm. Nitric acid (HNO_3, 70 wt%, Sigma-Aldrich), hydrogen peroxide (H_2O_2, 30% w/w, VWR Chemicals BDH), and hydrochloric acid (HCl, 37 wt%, Sigma-Aldrich) were used to prepare petcoke-derived acid catalysts. Methanol (MeOH, HPLC ≥ 99.9%, Sigma-Aldrich) and octanoic acid (OA, 99%, Thermo Scientific) were the reactants for the esterification reaction. A commercial solid-acid catalyst, Amberlyst-15 ion exchange resin (Thermo Scientific), was also tested for comparison to the petcoke-derived catalysts. A 0.1 N standard solution of sodium hydroxide (NaOH, J. T. Baker-Avantor), a 0.01 N standard solution of hydrochloric acid (J. T. Baker-Avantor), and phenolphthalein (1% w/v in 95% v/v Alcohol, RICCA Chemical Company) were utilized in the titration experiments to quantify total acidity.

Preparation of petcoke-derived solid acid catalysts. Before any treatment, PC and PCSi were wet ball milled using a Planetary Ball Mill (Pulverisette 6, Fritsch), with 5 mm zirconia balls at 300 rpm for 4 h at a sample-to-ball mass ratio of 1 : 25 (4 g of sample: 100 g of ZrO_2 balls) and 25 mL of isopropanol. The samples were dried in a vacuum drying oven at 65 °C to remove the isopropanol and named BPC and BPCSi, respectively. The ball-milled samples were functionalized with nitric acid as previously reported.[12,13] In a round-bottom flask, 5 g of BPCSi were mixed with 50 mL of HNO_3 and stirred at 600 rpm during refluxing at 90 °C for 8 h. Then, this mixture was filtered using a 0.22 μm membrane filter, and the solid was washed with reverse osmosis water and a 0.6 wt% HCl solution. After that, the solid was dried in a vacuum oven at 65 °C overnight to remove moisture and HCl, producing the BPCSi-HNO_3 catalyst. Functionalization with hydrogen peroxide was done for both BPCSi and BPC, and involved mixing 5 g of ball-milled petcoke with 50 mL of 30% w/w H_2O_2 followed by stirring at 600 rpm at room temperature for 20 h. The filtration, washing, and drying processes were conducted as previously described, producing the BPCSi-H_2O_2 and BPC-H_2O_2 materials.

Characterization. Thermogravimetric analysis (TGA, SDT Q600, TA Instruments, New Castle, DE, USA) was performed to determine the ash content and check the thermostability of the samples. Approximately 15 mg of material was heated under an air flow of 50 mL min^{-1} from ambient temperature to 750 °C at 20 °C min^{-1} and held at this temperature for 30 min. The structural properties of petcoke-derived catalysts were investigated by X-ray diffraction of powder samples (XRD, D8 Advanced ECO, Bruker, Bilerica, MA, USA), collected using a CuKα X-ray source, $\lambda = 0.15418$ nm, 2θ angles between 5 to 75°, 40 kV, and 25 mA. The samples were analyzed as received and loaded into a 25 mm polymethyl methacrylate (PMMA) sample holder. Chemical composition (CHNS) was determined by ultimate elemental analysis using a Flash 2000 CHNS analyzer (Thermo Scientific, Waltham, MA, USA). The morphology of the surface was investigated by scanning electron microscopy (SEM, Phenom Pro X, Thermo Fisher Scientific Phenom-World BV) at an acceleration voltage of 15 kV. Nitrogen adsorption and desorption isotherms were collected by N_2 physisorption at −196 °C using a Tristar II Plus analyzer (Micromeritics Instrument Corporation, Norcross, GA, USA), and the non-local density functional theory (NLDFT) model was used to determine surface area and pore volume. All samples were degassed at 150 °C under vacuum overnight before the analysis.

Surface functional groups on the samples were identified using a Fourier Transform Infrared (FTIR, Nicolet iS50, Thermo

Fisher Scientific, Waltham, MA, USA) spectrometer with attenuated transmission reflectance (ATR). The spectra were collected in the wavenumber range of 4000–400 cm^{-1}, at a resolution of 4 cm^{-1} and 128 scans. Additional surface analysis was performed by X-ray photoelectron spectroscopy (XPS, Kratos Axis Spectrometer, Kratos Analytical Limited, Manchester, UK) with monochromatized Al Kα ($h\nu$ = 1486.71 eV). Surface elemental compositions of the samples were obtained from the survey spectra, considering major elemental peaks. The peak fitting of components in the C 1s and S 2p narrow-scan spectra was done using CasaXPS (Version 2.3.22PR1.0, Casa Software Ltd, Teignmouth, UK), in which each component represents different chemical bonds. The peaks in the narrow scan spectra were fitted according to chemical and physical constraints.[16,42] For the C 1s fitting, the constraints applied were the same FWHM for all peaks (0.8–1.8 eV), with peak position as reported in literature,[13,43–45] with a shift of ±0.3 eV for each component. While the fitting of peaks for the S 2p narrow scan followed the approximate 2 : 1 relative area of the spin–orbit doublets ($2p_{3/2}$ and $2p_{1/2}$) for each species, separated by 1.18–1.2 eV with equal FWHM (1.2–1.6 eV), and peak position as reported in literature.[44–51] The total acidity (number of total surface acidic groups) on the petcoke-derived catalysts was determined using a modified Boehm titration method. A mixture of 0.05 g of sample and 5 mL of a 0.1 N NaOH standard solution was oscillated in a shaker at 25 °C, 250 rpm for 24 h. Then, 1 mL of this solution was filtered and back-titrated with a 0.01 N standard solution using phenolphthalein as indicator.

Esterification reaction. The esterification reactions between octanoic acid and methanol were performed in a 100 mL two-neck round-bottom flask connected to a reflux condenser. The system was heated in a water bath and constantly stirred at 850 rpm. For a typical run, the methanol to octanoic acid molar ratio used was 10 : 1 (~23.0 g of MeOH and ~10.0 g of OA), mixed with ~0.5 g of catalyst (5 wt% of OA) for 6 h at 60 °C. Periodically (every 30 min to 90 min then every 60 min), 0.2 mL samples were withdrawn from the mixture and filtered with a membrane filter (0.22 μm, nylon) to remove the solid catalyst. Once withdrawn, the solution cooled to room temperature at which the rates of the heterogeneous and homogeneous reactions were negligible. A fraction of the withdrawn sample (44 μL of solution) was diluted in 10 mL of methanol and quantified by gas chromatography with Flame Ionization Detection (GC-FID, 8860 GC-FID, Agilent Technologies, Santa Clara, CA, USA) using a DB-FATWAX UI (polyethylene glycol-type, 30 m × 0.25 mm × 0.25 μm) capillary column. The temperature program of the GC consisted of 0.5 min at 50 °C, then a ramp of 40 °C min^{-1} to 200 °C, holding for 2 min. Helium (He) was used as the carrier gas, in which an aliquot of 1 μL of each sample was injected in the split mode (ratio of 100 : 1), with an inlet temperature of 250 °C. The detector mode was at a constant makeup flow of 25 mL min^{-1} of He, 450 mL min^{-1} of air, and 40 mL min^{-1} of hydrogen (H_2). The samples were analysed in triplicate, and the error of the analysis was estimated to be <1%. The only chemicals identified by GC-FID were octanoic acid (OA) and methyl octanoate (MOA).

The ester yield was calculated based on the following equation:

$$\text{Ester Yield}(\%) = \frac{[\text{MOA}]_{\text{actual}}}{[\text{MOA}]_{\text{theoretical}}} \times 100\% \quad (1)$$

where $[\text{MOA}]_{\text{actual}}$ is the concentration of methyl octanoate formed and $[\text{MOA}]_{\text{theoretical}}$ is the theoretical maximum concentration of ester, which is equal to the initial concentration of octanoic acid. The initial turnover frequencies (TOF), which represent the catalyst activity per site, were calculated as follows:[13]

$$\text{TOF}(h^{-1}) = \frac{k \times [\text{OA}]_0 \times V}{m_{\text{catalyst}} \times [-SO_3H]} \quad (2)$$

where k is the pseudo first-order rate constant (h^{-1}), $[\text{OA}]_0$ is the initial concentration of octanoic acid (mmol mL^{-1}), V is the total volume of the reaction solution (mL), m_{catalyst} is the mass of catalyst utilized in the reaction (g), and $[-SO_3H]$ is the concentration of sulfonic acid sites on the catalyst surface (mmol g^{-1}). Eqn (3) shows the pseudo first-order model, which assumes a constant methanol concentration and negligible reverse reaction rate:[10,52]

$$[\text{OA}] = [\text{OA}]_0 e^{-kt} \quad (3)$$

where [OA] is the concentration of OA (mmol mL^{-1}) at time t (h) and k is the rate constant (h^{-1}) for the pseudo first-order model, in which all assumptions were satisfied with the conditions applied at the initial stages of the reaction.

Catalyst reuse and regeneration. To evaluate the stability of the catalysts, a reuse experiment was performed with the spent catalyst recovered after the first reaction cycle. After the reaction, the catalyst was filtered, washed with methanol to eliminate any chemical adsorbed on the surface of the material, and dried overnight in the fume hood. Then, the catalyst was used again for the esterification reaction under the same conditions previously described.

For the regeneration of catalysts, the procedure was modified from the literature.[53] The deactivated material (after the first cycle) was washed with methanol and acetone. Then, the catalyst was immersed in 50 mL of 1 M H_2SO_4 solution for 24 h and stirred at room temperature. After that, the catalyst was filtered and washed with reverse osmosis water until the residual solution reached pH 7. The samples were dried in a vacuum oven at 60 °C overnight before being used in the esterification reaction once more.

Results and discussion

Esterification reaction

Fig. 1 shows the catalytic activity of the petcoke-derived solid acid catalysts prepared by chemical treatment with nitric acid or hydrogen peroxide in the esterification reaction of octanoic acid and methanol. Each ester yield data point is an average of 3 runs, and the error bars represent one standard deviation. Without functionalization, PCSi, and the ball-milled sample (BPCSi) were inactive for the esterification reaction, and the

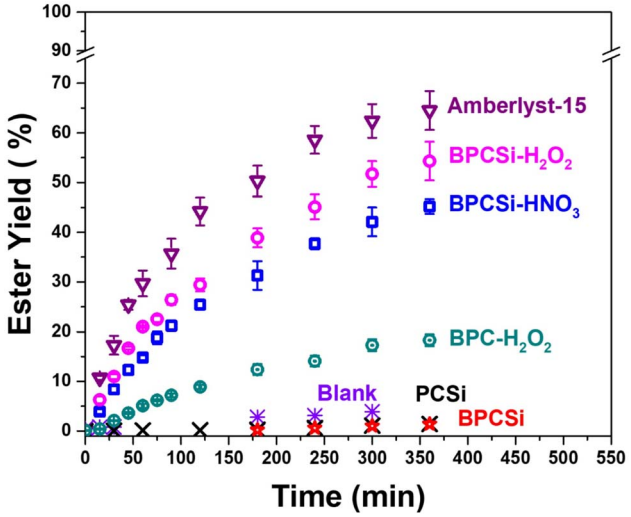

Fig. 1 Esterification of octanoic acid using petcoke-derived catalysts. Reaction conditions: MeOH : OA molar ratio = 10 : 1, 5 wt% of catalyst (based on the weight of octanoic acid), 60 °C, 800 rpm.

ester yield obtained in both cases (1.5%) were lower than the blank test (4.4%). The blank test results indicate that there was a relatively slow homogeneous reaction occurring. The lower yield obtained in the presence of PCSi and BPCSi can be explained by the adsorption of the product, from the homogeneous reaction, on the oxygen-containing carbon groups (*i.e.*, hydroxyl and ether groups) on the surface of petcoke.[13]

After chemical treatment, the activity improved in the order of samples BPC-H_2O_2 < BPCSi-HNO_3 < BPCSi-H_2O_2, with ester yields after 6 h of 17%, 45%, and 55%, respectively. All prepared materials had a lower yield than the 65% yield obtained with the commercial Amberlyst-15 catalyst. Ester yields negatively correlate with the number of oxygen-containing carbon functional groups on the petcoke-derived catalyst surface,[13] which might explain the poorer performance of BPCSi-HNO_3. The performance of the high silica-containing petcoke was over three times better than that of the petcoke with a lower silica content. Table S1 summarizes other recent studies on waste-derived carbon-based solid acid catalysts, with a series of materials prepared *via* the extensively studied sulfonation with sulfuric acid (H_2SO_4),[10,22–24,26] applied in the esterification reaction of octanoic or oleic acid with methanol. The difference between these carboxylic acids is their carbon chain length – oleic acid has 18 carbons and octanoic acid has only 8 carbons. The reactivity of these molecules, under the same conditions, decreases with the growth of the carbon chain due to steric hindrance.[54] So, a material that is active for the esterification of oleic acid should be more active for the reaction with octanoic acid. The estimated TOF for BPCSi-H_2O_2 (308 h^{-1}) and BPCSi-HNO_3 (192 h^{-1}) were higher than the other waste-derived materials (between 1.3–68 h^{-1}) and Amberlyst-15 (6 h^{-1}). The fact that higher yields were reported for these catalysts[21–24,26] suggests that an excess of catalyst was used in the experiments. In addition, the reaction conditions were different with higher temperatures,[21–23] and a higher excess of alcohol.[10,22,23] Comparing the TOFs, the activity per site of the –SO_3H groups originated from the inherent sulfur species in petcoke is better than that on the surface of Amberlyst-15, and that generated from sulfonated waste-derived carbon materials.

Even though the chemical functionalization of petcoke with hydrogen peroxide produced a more active material than the nitric acid treatment, the catalyst stability was not improved (Fig. 2 and S1). All samples, including Amberlyst-15, were deactivated after the first cycle. The deactivation was more pronounced for the petcoke-derived solid acid catalysts, for which the ester yields decreased to 10–15%. This loss in activity could be due to the partial deactivation of acid sites or the leaching of sulfonic acid sites into the solution.[53,55] The

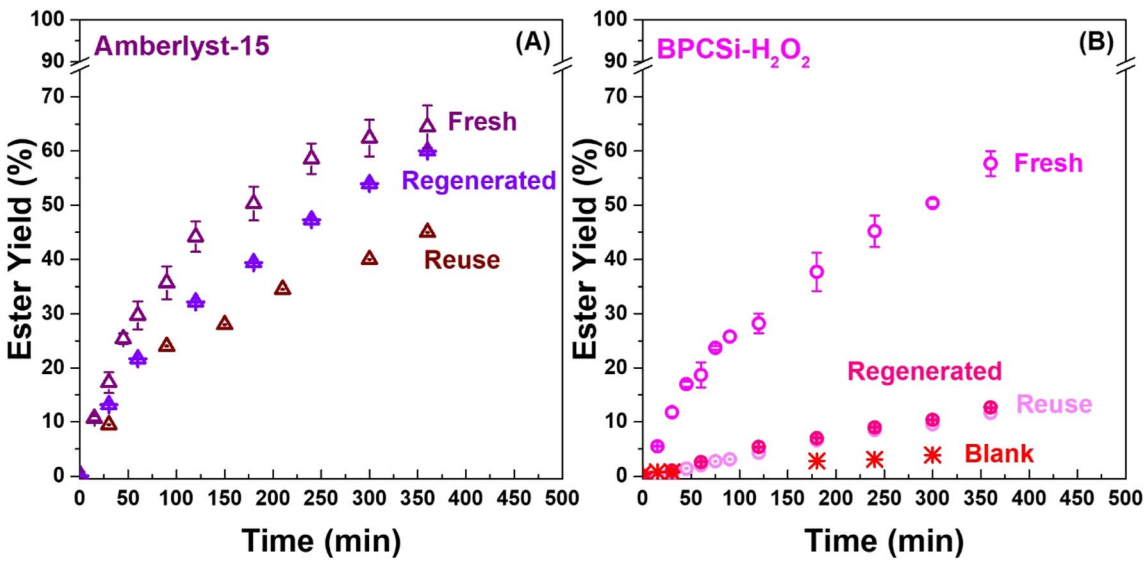

Fig. 2 Esterification of octanoic acid using fresh catalyst, spent catalyst (reuse curve), and catalyst after regeneration with H_2SO_4: Amberlyst-15 (A) and BPCSi-H_2O_2 (B). Reaction conditions: MeOH : OA molar ratio = 10 : 1, 5 wt% of catalyst, 60 °C, 800 rpm.

performance of the regenerated catalysts is shown in Fig. 2. The deactivation of the Amberlyst-15 was reversible, and the majority of the activity could be recovered after acid treatment (Fig. 2A). The BPCSi-H_2O_2 catalyst, however, was irreversibly deactivated, consistent with leaching of sulfonic acid sites (–SO_3H) to the reaction solution. These results are consistent with those of other waste-derived carbon-based materials (Table S1). Sulfonated activated carbon from coffee residue[25] and from spent coffee grounds[26] lost ~70% of their initial activity after the 5th and 4th cycle, respectively, which is comparable with the loss for BPCSi-HNO_3 and BPCSi-H_2O_2 after the 2nd use. Again, the reaction conditions and amounts of catalyst used were different in each study. Catalysts that are more porous may have active sites that take longer to diffuse through the material and into solution, as well as more active sites per mass of catalyst. For example, the loss of activity for the higher porosity materials (*i.e.*, activated carbon) made from potato peel,[22] ginger straw,[23] and garlic peel[24] was lower (~30% of the initial ones) after 4 to 5 cycles, but still significant. The sulfonated activated carbon produced from corn cob,[21] with the highest porosity and initial –SO_3H concentration, had the lowest loss in activity of only 9% after 8 cycles. The higher TOF observed for BPCSi-HNO_3 and BPCSi-H_2O_2 may originate from the faster detachment of –SO_3H groups from the surface for these lower porosity materials (Table 1). The rate of the homogeneous reaction contributes to the overall activity of the system but is not considered in most studies. In this study, it is not known if the sulfonic acid sites catalyze the esterification of octanoic acid before detaching from the surface. While the sites are not stable in methanol (leaching tests), in the presence of the reactant (octanoic acid), the material may act as a solid acid catalyst.

Table 1 Surface area, pore volume, and ash content of petcoke before and after functionalization with different agents

	N_2 physisorption		
Sample	Surface area ($m^2\ g^{-1}$)	Pore volume ($cm^3\ g^{-1}$)	Ash (wt%)
PCSi	1	0.008	47.5
BPCSi	23	0.068	48.2
BPCSi-HNO_3	20	0.084	37.7
BPCSi-H_2O_2	26	0.082	44.7
PC	1	0.004	6.9
BPC	2	0.008	10.5
BPC-H_2O_2	2	0.007	14.2

Catalysts properties: differences between functionalization with HNO_3 and H_2O_2

The XRD patterns and FTIR spectra of petcoke before (PCSi) and after functionalization with HNO_3 and H_2O_2 are shown in Fig. 3. In the XRD analysis, a broad peak at $2\theta \approx 25.0°$, characteristic of petcoke, and corresponding to the graphite C (002) plane, is evident. In addition, several sharp peaks at 2θ = 21°, 26.6°, 36.6°, 39.6°, 40.4°, 42.6°, 45.6°, 50.2°, 55.1°, 60.0, and 67.9° are present, which are attributed to the crystalline structure of SiO_2. Moreover, PCSi and BPCSi-H_2O_2 samples have a peak at 2θ = ~12°, which is characteristic of the kaolinite mineral structure ($Al_2Si_2O_5(OH)_4$).[56–58] This mineral is usually present in silica sand composition[56] and has been reported as one of the minerals in Alberta oil sands.[58] The relative intensities of these peaks between samples are consistent with the ash values shown in Table 1, which contains the physical properties of the materials. Due to the high intensity of the SiO_2 diffraction peaks, it was not possible to observe any differences in the structure of the petcoke-derived catalysts after chemical functionalization. These results are consistent with previous findings[59] where a blend of petcoke and SiO_2 with a carbon-to-silicon elemental ratio of 1 : 1 had only SiO_2 peaks in the XRD pattern.

The surface area and pore volume were calculated from N_2 physisorption experiments. After the functionalization of PCSi,

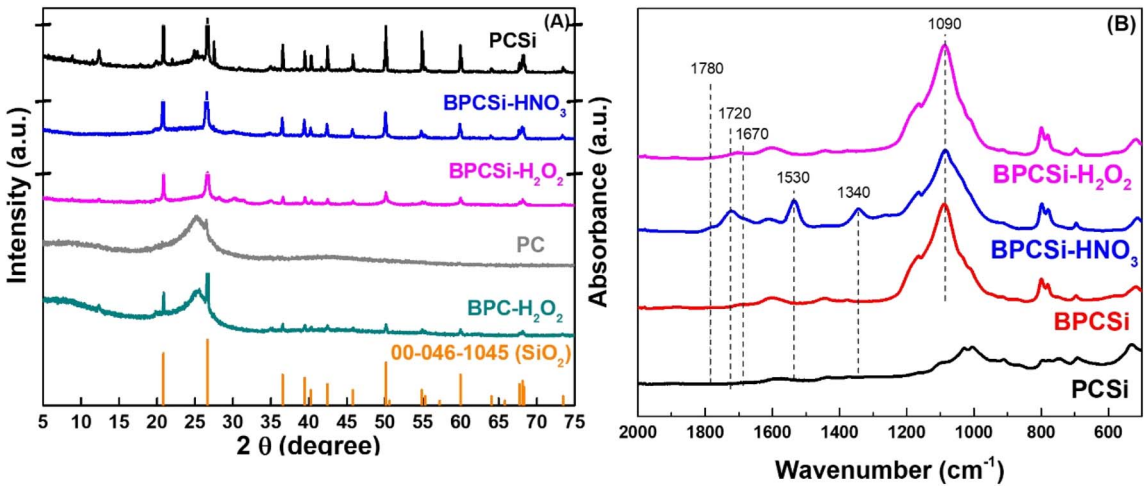

Fig. 3 Characterization of bulk and surface properties of petcoke-derived samples. (A) XRD patterns of catalysts and reference pattern for SiO_2 (PDF-5+ card of quartz). The peaks at 21° and 26.6° of PCSi, BPCSi-HNO_3, and BPCSi-H_2O_2 samples were truncated to enhance visibility of minor peaks; (B) ATR-FTIR spectra of high silica petcoke before and after functionalization with different agents.

there was an overall increase in the surface areas and pore volumes of the prepared samples (BPCSi-H_2O_2 and BPCSi-HNO_3), but these materials are much less porous than activated carbon. The decrease in ash content (Table 1 and Fig. S2) for BPCSi-HNO_3 (38%) when compared to PCSi (47.5%) was likely due to the removal of some mineral impurities during the treatment with nitric acid,[13] which is reinforced by the absence of a diffraction peak at $2\theta = \sim 12°$ for this sample. In contrast, no significant change in ash content was detected for BPCSi-H_2O_2 (45%). Overall, there were not many differences between the physical properties of BPCSi-HNO_3 and BPCSi-H_2O_2, so the better activity for the latter is related to its chemical properties.

The S/C and O/C ratios were calculated using the ultimate elemental analysis of the catalysts (Table S2) – the PCSi sample had an S/C of 0.073 and O/C of 0.03. After functionalization with both hydrogen peroxide and nitric acid, there was a slight decrease in S/C ratio to 0.062 and 0.071 for BPCSi-HNO_3 and BPCSi-H_2O_2, respectively. The major change was in the O/C ratio of BPCSi-HNO_3 that increased to 0.47, while that of BPCSi-H_2O_2 increased only marginally from 0.03 to 0.06. After the functionalization with HNO_3 and H_2O_2, the concentration of oxygen was expected to increase due to the formation of sulfonic acid sites and other oxygen-containing carbon functional groups, consistent with the increased O/C ratio for both samples.

The chemical states of functional groups after HNO_3 and H_2O_2 functionalization were investigated by FTIR (Fig. 3B) and XPS (Fig. 4). The FTIR spectrum of PCSi had a band centered at 1600 cm^{-1} associated with poly-aromatic rings of hydrocarbon molecules and bands between 900–600 cm^{-1}, which correspond to aromatic hydrogen.[10] After functionalization, the infrared spectra of BPCSi-HNO_3 and BPCSi-H_2O_2 had absorption bands at 1670, 1720, and 1780 cm^{-1} assigned to C=O stretching of –COOH, C–O, and C=O groups,[60,61] and vibration in the region of 1280–940 cm^{-1}. Although these spectra have intense bands at ~1030 cm^{-1} and ~1200 cm^{-1}, which are related to the S=O stretching vibration of sulfonic groups,[12,13,18] the $-SO_3H$ formation could not be confirmed using only the FTIR technique. Silica has Si–O–Si vibration absorption between 1200–1000 cm^{-1} [62,63] that overlaps with the sulfonic acid functional group. The FTIR spectrum of silica is shown in Fig. S3, confirming that the peaks between 1200–1000 cm^{-1} in the FTIR spectra of BPCSi and the functionalized materials are mainly due to the presence of SiO_2. Also, after ball-milling treatment, the peak intensity of Si–O–Si stretching vibration increased when compared to PCSi (Fig. S3). This behaviour has also been reported for biochar made from sugarcane bagasse and wheat straw after ball-milling and is associated with the high silica content of these materials.[64] The acid-treated catalyst (BPCSi-HNO_3) had the most intense bands of C=O stretching as well as bands at 1340 cm^{-1} and 1530 cm^{-1} associated with NO_2 stretching modes, indicating the presence of nitro groups.[13] Moreover, the FTIR results suggested that this material has

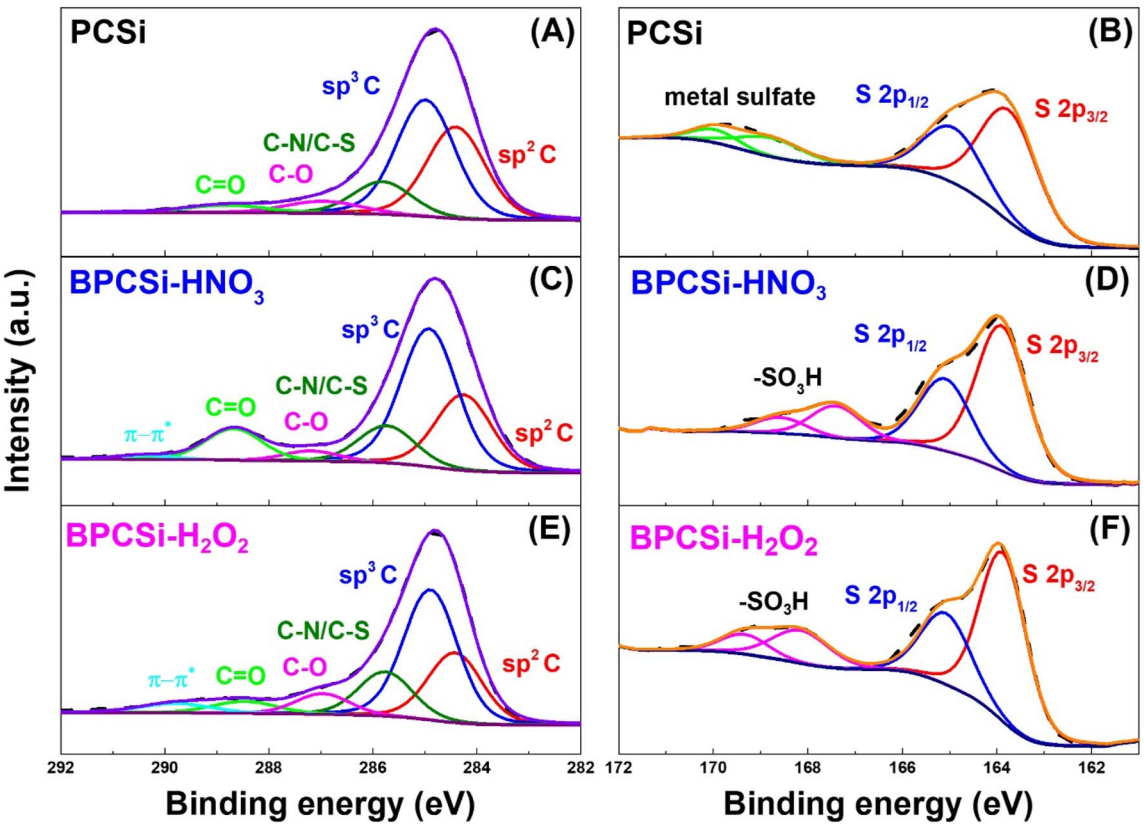

Fig. 4 Narrow scan XPS spectra for pristine high-silica petcoke (PCSi) and after ball-milling and functionalization with HNO_3 and H_2O_2 C 1s (left-A, C, E) and S 2p (right-B, D, F).

more oxygen-containing groups on its surface than BPCSi-H_2O_2, which may explain the poorer activity of BPCSi-HNO_3.

The surface properties of the petcoke-derived catalysts were also analyzed by X-ray photoelectron spectroscopy (XPS). The surface elemental composition was calculated in weight percentage from the survey spectra (Fig. S4), and the results are shown in Table S3. In addition to carbon, oxygen, nitrogen, and sulfur, two other elements were detected on the surface of petcoke-derived samples: silicon and aluminium. PCSi contained 16.6 wt% Si. After treatment, BPCSi-HNO_3 had an increase in the nitrogen content, as expected, and an increase in the O/C ratio (from 0.50 to 0.76) while the S/C ratio did not significantly change. The significant decrease in the Si/C and Al/C ratio after acid functionalization is consistent with mineral impurity removal (*i.e.*, lower ash content, Table 1). The petcoke functionalization with hydrogen peroxide, on the other hand, resulted in a material (BPCSi-H_2O_2) with a lower sulfur content on the surface, demonstrated by the decrease in S/C ratio. This decrease is likely due to partial oxidative desulfurization promoted by H_2O_2 during preparation,[65,66] and an increase in the O/C ratio (from 0.50 to 0.89). The greater O/C ratio for BPCSi-H_2O_2 was associated with the higher SiO_2 content in this sample, as demonstrated by its ash percentage and more intense peaks in FTIR related to Si–O–Si vibration (Fig. 3B). In addition, the higher Si/C and Al/C ratios for this sample were related to a reduction in the carbon content after functionalization, and not to mineral removal.

The fitting of peaks for the XPS narrow scan spectra are shown in Fig. 4 and were used to determine the oxidation states of carbon and sulfur in the samples. The C 1s spectra (Fig. 4A, C, and E) contained five peaks for the PCSi sample, centred at 284.9 eV, 284.4 eV, 285.8 eV, 287.0 eV, and 288.7 eV corresponding to sp^3 carbon, sp^2 carbon, carbon hybridized with N and S, C–O, and C=O,[13,43–45] respectively. After functionalization with HNO_3 and H_2O_2, one additional peak was detected centered at ~290 eV corresponding to π–π* transition (O=C–O), indicating the addition of oxygen-containing carbon groups on the surface. The percentage of carbon in the C–O bond changed from 5.6% for PCSi to 3.4% for BPCSi-HNO_3, and 7.1% for BPCSi-H_2O_2. The C=O bond content increased from 3.8% in petcoke (PCSi) to 10.7% for BPCSi-HNO_3 and 5.4% for BPCSi-H_2O_2 (Table S4). The sulfur species are shown in Fig. 4B, D, and F, and the PCSi S 2p spectrum was fitted into four peaks, corresponding to two different species. The peaks centred at 163.9 eV and 165.0 eV are attributed to C–S–C ($2p_{3/2}$ and $2p_{1/2}$, respectively), characteristic of sulfur in the thiophene structure,[46,47] while the peaks at ~169 eV and 170 eV are the binding energy of SO_4^{2-} species related to metal sulfates in petcoke.[48–50] After functionalization, the sulfate peak disappeared, and two additional peaks at 167.7 eV and 168.8 eV related to –SO_3H groups[44,45,51] appeared in the S 2p high-resolution spectra of BPCSi-HNO_3 and BPCSi-H_2O_2. This result confirmed that hydrogen peroxide can access and convert the inherent sulfur species in petcoke into sulfonic acid sites, in the same way as has been demonstrated for nitric acid.[12] Even though BPCSi-HNO_3 had a higher concentration of oxygen groups, as demonstrated by elemental analysis, the XPS spectrum was not significantly different from BPCSi-H_2O_2. The main difference was in the C=O intensity, which is higher for the former in accordance with the FTIR results.

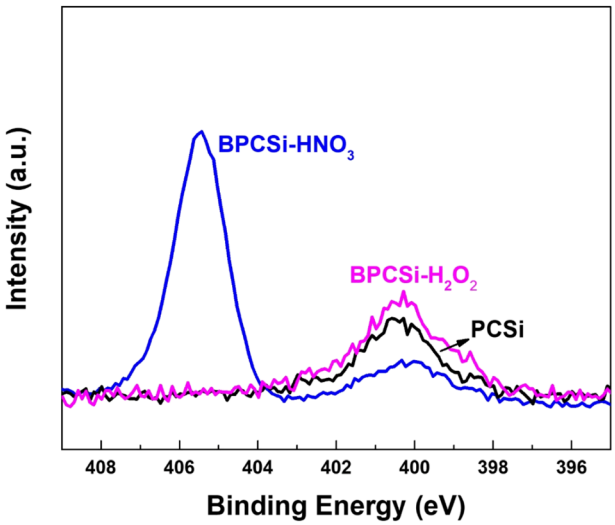

Fig. 5 Narrow scan XPS spectra of N 1s for PCSi and petcoke-derived solid acid catalysts.

The N 1s narrow scan spectra of PCSi and chemically treated samples are shown in Fig. 5. Before (PCSi) and after functionalization with hydrogen peroxide (BPCSi-H_2O_2), the amount of nitrogen on the surface was ~1 wt% (Table S3), and one broad peak centered at ~400.0 eV can be seen and is reported as N–O, pyrrolic or pyridinic structures.[67,68] The nitric acid treatment resulted in the increase of nitrogen content on the surface (3.6 wt%) due to the formation of nitro groups (–NO_2) demonstrated by the additional peak at the binding energy of 405.5 eV[13,68] and confirmed by the FTIR results of the BPCSi-HNO_3 samples (Fig. 3B).

The number of total surface acidic groups on the samples was calculated using the Boehm titration method, and the concentration of sulfonic acid sites was estimated based on the XPS results, as shown in Table 2. Initially, PCSi had no sulfonic acid sites on the surface, based on XPS, and a low total acidity of 0.30 mmol g^{-1}. After the ball milling treatment, the total acidity of the resulting sample (BPCSi) increased to 0.67 mmol g^{-1}. This increase in the total acidity was due to the exposure of silanol groups (Si–OH) on the surface of silica sand, which is a common effect when in contact with water[69] – isopropanol applied in the ball-milling process is hygroscopic. The ATR-FTIR spectra of BPCSi (Fig. S5B) had a band at ~3450 cm^{-1} attributed to the vibration of Si–OH groups.[70] Functionalization with nitric acid generated a catalyst (BPCSi-HNO_3) with an increased total acidity of ~5 mmol g^{-1} and a 0.14 mmol g^{-1} concentration of –SO_3H sites. The petcoke functionalization with hydrogen peroxide resulted in a material (BPCSi-H_2O_2) with a much lower total acidity (1.29 mmol g^{-1}), and a lower density of sulfonic acid sites (0.09 mmol g^{-1}).

The XPS C 1s and S 2p narrow scan spectra of the spent catalysts produced from a high-silica petcoke are shown in Fig. 6. After use, the sulfonic acid sites on the surface of BPCSi-

Table 2 Acidity and turnover frequency (TOF) of Amberlyst-15, petcoke, and functionalized petcoke

	Acidity (mmol g^{-1})		Fresh catalyst		Reused catalyst
Sample	$[-SO_3H]^a$	Total[b]	Ester yield[c] (%)	TOF (h^{-1})	Ester yield[c] (%)
Amberlyst-15	4.70[f]	4.70[f]	64.5	6	44.8
PCSi	0	0.30 ± 0.14	1.5	—[d]	—[e]
BPCSi	0	0.67 ± 0.06	-[e]	—[d]	—[e]
BPCSi-HNO_3	0.14	5.01 ± 0.21	45.1	192	16.1
BPCSi-H_2O_2	0.09	1.29 ± 0.26	54.2	308	17.2
PC	0	0.24 ± 0.04	—[e]	—[d]	—[e]
BPC	0	0.33 ± 0.06	-[e]	—[d]	—[e]
BPC-H_2O_2	0.20	0.97 ± 0.04	17.3	42	—[e]

[a] Estimated from XPS spectra. [b] Estimated by Boehm titration. [c] After 6 h. [d] Not calculated for materials without $-SO_3H$ acidity. [e] Not determined. [f] From the product data sheet of the manufacturer. In Amberlyst-15 all the acidity is attributed to acid sulfonic acid groups.

HNO_3-spent were completely gone, as demonstrated by the absence of $-SO_3H$ peaks in the narrow scan S 2p spectra of this sample (Fig. 6B) and a decrease in the sulfur content on the surface of this catalyst from 2.5 wt% in the fresh sample to 0.6 wt% in the spent material (Table S5), demonstrating the complete leaching of $-SO_3H$ sites during the esterification reaction. The BPCSi-H_2O_2-spent, on the other hand, still presented peaks at ~168.0 eV and ~169.0 eV corresponding to sulfonic acid sites. However, the total sulfur concentration decreased considerably from 1.4 wt% to 0.7 wt% (Table S5), also indicating leaching of the active sites, but not completely as for BPCSi-HNO_3-spent. For comparison, the density of sulfonic acid sites in the fresh sample was 0.09 mmol g^{-1}, which decreased to 0.03 mmol g^{-1} for the spent material. The C 1s narrow scan spectra of the spent samples were similar to the fresh ones, and the distribution of functional groups did not significantly change (Table S6).

Although BPCSi-H_2O_2 had a lower concentration of $-SO_3H$ sites than BPCSi-HNO_3, the former had a higher activity per site (TOF) of 308 h^{-1} *versus* 192 h^{-1} for the nitric acid catalyst. The lower activity of BPCSi-HNO_3 can be attributed to its higher total acidity, which includes contributions from acidic oxygen-containing carbon groups such as lactonic and carboxylic functionalities,[71] as demonstrated by the FTIR bands at 1670,

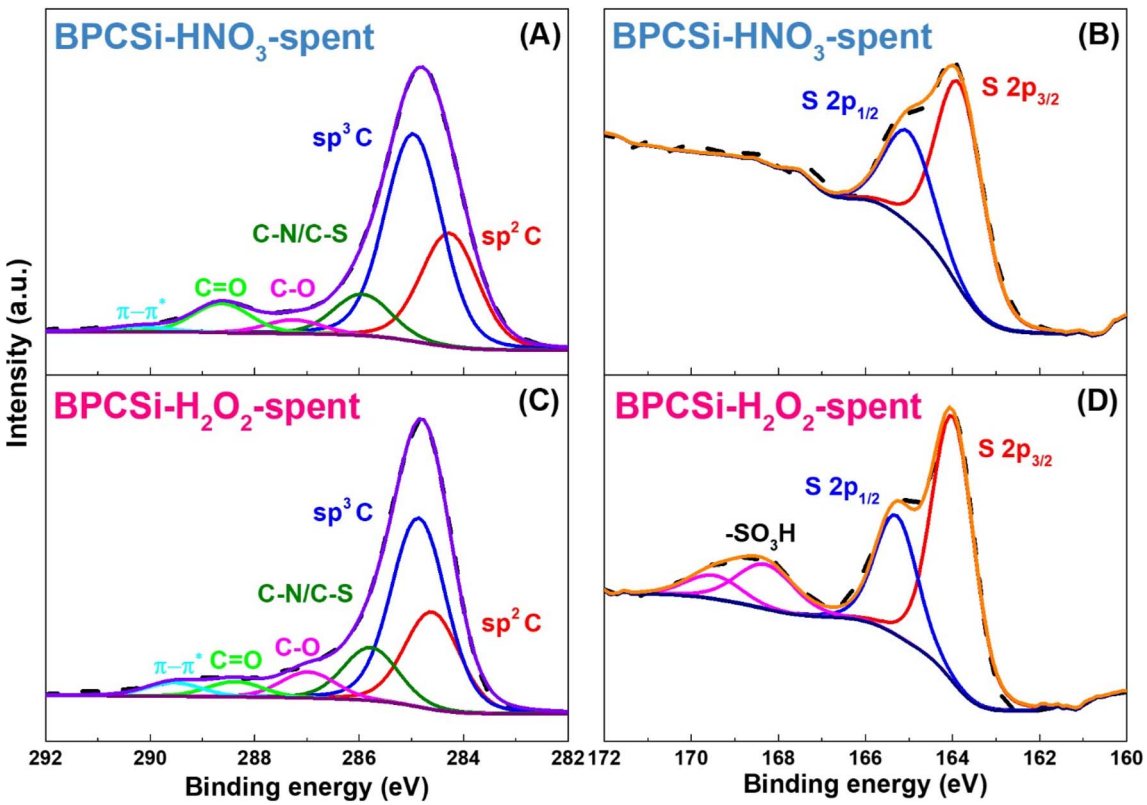

Fig. 6 Narrow scan XPS spectra for spent catalysts prepared from a high-silica petcoke C 1s (left-A and C) and S 2p (right-B and D).

1720, and 1789 cm^{-1} (Fig. 3), as well as a small contribution of the silanol groups. The oxygen-containing carbon groups hinder the reaction by promoting the adsorption of reactants and products through hydrogen bonding interactions, particularly with methanol, octanoic acid, and the ester formed, causing steric hindrance.[13,72,73] In addition, the TOF calculation was done in terms of the sulfonic acid site concentration only, because these oxygen-containing carbon groups present weak acidity that cannot protonate the carboxyl group of the octanoic acid, which is the first step of the reaction. This protonation requires strong Brønsted acid sites; therefore, only $-SO_3H$ groups are considered truly active sites for the reaction.[55,74–78]

Therefore, the functionalization with hydrogen peroxide resulted in a more active catalyst than the functionalization with nitric acid because of the formation of fewer oxygen-containing carbon groups on the surface of BPCSi-H_2O_2 when compared to BPCSi-HNO_3. This observation supports the hypothesis that enhancing the activity of petcoke-derived catalysts is highly dependent on a reduction in the number of oxygen-containing carbon groups formed during material preparation. Specifically, these groups seem to negatively influence the catalyst activity to a much greater extent than the positive effect of a higher concentration of sulfonic acid sites. Ideally, to achieve even better catalytic performance with these petcoke-derived materials, it is desirable to keep the total acidity as low as the one obtained for BPCSi-H_2O_2, while promoting the formation of additional $-SO_3H$ groups. The maximum possible concentration of sulfonic acid sites was calculated to be 0.83 mmol g^{-1}, assuming that all sulfur in PCSi was converted to $-SO_3H$. Thus, there is potential for improvement, as only about 10% of this maximum value has been achieved with BPCSi-H_2O_2.

Catalyst properties: effect of initial SiO_2 content on the petcoke feedstock

The presence of silica in the petcoke feedstock arises from different stages of production, processing, and handling. During the coking step, the equipment used (siliceous refractory linings) and silica-based additives applied in the process might contribute to the silica content in the final product.[34,35] More than likely, however, the major contribution comes from handling and storage. Petcoke is largely stockpiled in an open field,[29–31] in direct contact with the ground. If the storage area is rich in silica sand, and precautions are not taken, SiO_2 can get mixed with petcoke. The area from which the petcoke used in this study was obtained (Fort McMurray – Alberta, Canada) is abundant in silica sand.[79] So, a batch of petcoke from the bottom of the pile can have a much higher fraction of sand mixed with it.

The esterification results (Fig. 1) showed that BPCSi-H_2O_2, generated from a feedstock containing a higher silica content (PCSi), was much more active than BPC-H_2O_2. Both samples were prepared in the same way, and silica (SiO_2) is generally chemically inert at the reaction conditions used in this study.[80] Thus, the results suggest that while the SiO_2 component does not directly catalyze the esterification reaction, it contributes to enhancing the activity of the resulting catalyst. To investigate how silica sand is affecting the overall performance of petcoke-derived samples in the esterification reaction, the structural properties of hydrogen peroxide-treated materials were investigated by XRD (Fig. 3). PC has the characteristic broad peak at $2\theta = 25°$ related to graphite C (002), and a sharp peak at 26.6° 2θ corresponding to microcrystals of SiO_2. After ball milling and H_2O_2 functionalization (BPC-H_2O_2), the SiO_2 crystalline structure, as well as the kaolinite characteristic peak, became more evident and reflect the increase in the ash content from 6.9 wt% for PC to 14.2 wt% for BPC-H_2O_2 (Table 1), suggesting that part of the carbon is decomposed during the chemical functionalization process. The difference between the XRD patterns of BPC-H_2O_2 and BPCSi-H_2O_2 is mainly the intensity of SiO_2 peaks, which does not explain the better performance of the latter.

The ultimate elemental analysis of PCSi and PC (Table S2) revealed similar S/C (0.073 and 0.076, respectively) and O/C (0.03 and 0.01, respectively) ratios for both samples, corroborating the existence of SiO_2 as a physical mixture in PCSi. The surface chemical groups of PC and BPC-H_2O_2 were investigated by FTIR-ATR (Fig. S5) and XPS C 1s and S 2p high-resolution spectra (Fig. S6). The functional groups existing on the surface of the materials before and after functionalization with hydrogen peroxide were the same as those of PCSi and BPCSi-H_2O_2, respectively. Even the distribution of carbon species (sp^2 C, sp^3 C, C–N/C–S, C–O, C=O, and π–π*) and sulfur species (C–S–C, C=S, $-SO_3H$, and SO_4^{2-}) in Table S4 were quite similar for BPC-H_2O_2 and BPCSi-H_2O_2, suggesting that SiO_2 has no influence on the oxidation pathway of petcoke. After functionalization with hydrogen peroxide, the S/C ratio decreased and the O/C, Si/C, and Al/C ratios increased for both BPCSi-H_2O_2 and BPC-H_2O_2 (Table S3).

Comparing the number of total surface acidic groups and the density of sulfonic acid sites (Table 2) of the hydrogen peroxide-treated samples, BPC-H_2O_2 showed a total acidity of 0.97 mmol g^{-1} and sulfonic acid sites concentration of 0.20 mmol g^{-1}. The BPCSi-H_2O_2 sample had values of 1.29 mmol g^{-1} and 0.09 mmol g^{-1} (total and $-SO_3H$, respectively). The total acidity, which is mainly related to the oxygen-containing carbon groups, of both samples is similar, and the density of sulfonic acid sites is twice as high for BPC-H_2O_2. From these results, it was expected that the activity of this catalyst would be much higher than BPCSi-H_2O_2. On the contrary, the TOF of BPCSi-H_2O_2 is sevenfold better than BPC-H_2O_2 (308 h^{-1} compared to 42 h^{-1}, respectively). Although the concentration of sulfonic acid sites in BPC-H_2O_2 is higher than in BPCSi-H_2O_2, normalization by the SiO_2 content in each sample (ash% in Table 1) yields comparable values, indicating that the presence of silica did not significantly affect the resulting concentration of sulfonic groups. Also, the reuse test of BPC-H_2O_2 (Fig. S1), XPS S 2p spectrum of the spent catalyst (Fig. S7), and sulfur content on its surface (Table S5) showed a leaching of $-SO_3H$ groups after the first cycle. The fresh catalyst had a sulfur content of 3.0 wt% that decreased to 1.9 wt% in the spent material, representing a significant loss in sulfonic acid site concentration that resulted in a density of 0.06 mmol g^{-1} in BPC-H_2O_2-spent – much lower than the

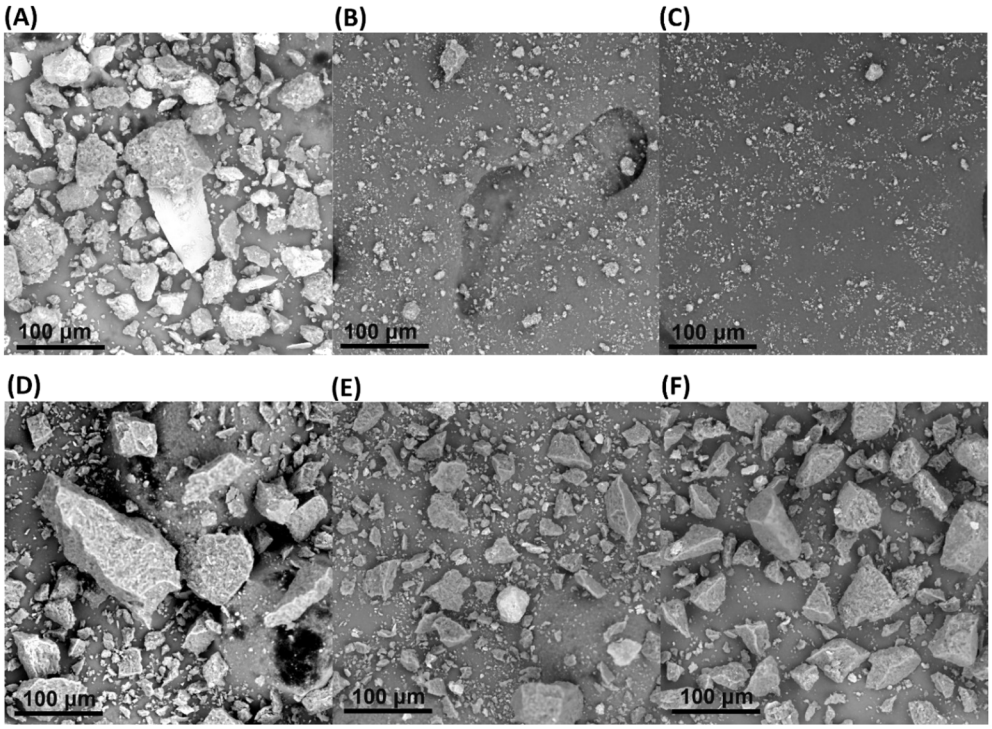

Fig. 7 SEM images PCSi (A), BPCSi (B), BPCSi-H_2O_2 (C), PC (D), BPC (E), and BPC-H_2O_2 (F). Brighter particles are silica sand (SiO_2).

0.20 mmol g^{-1} in the fresh material (BPC-H_2O_2). If all the sulfonic acid sites were on the surface of BPC-H_2O_2 and were leached to the reaction solution, this material would have a higher activity than BPCSi-H_2O_2 – considering the higher sulfonic acid sites density of the former. Therefore, a fraction of $-SO_3H$ groups in the BPC-H_2O_2 samples was likely to be inaccessible for the reaction of octanoic acid molecules. Comparing the total acidity of the BPCSi (0.67 mmol g^{-1}) and BPC (0.33 mmol g^{-1}), however, the presence of a higher content of SiO_2 generates more silanol groups that have a weak acidity, behaving as hydrogen-bond donors[81,82] that facilitate the protonation of the octanoic acid and methanol, but the silanol groups alone were not active in the esterification reaction, as the ester yield of BPCSi after 6 h was only 1.5% (Fig. 1). Therefore, the hydrogen-bond donation effect of silanol groups alone could not be responsible for such a difference in the performance between BPCSi-H_2O_2 and BPC-H_2O_2.

The SEM images of PCSi, BPCSi, BPCSi-H_2O_2, PC, BPC, and BPC-H_2O_2 are shown in Fig. 7. Initially, PCSi and PC were sieved into particles of 20–100 μm (Fig. 7A and D, respectively). After the ball-milling process, a significant reduction of particle size was noticeable for the feedstock containing a higher silica content (Fig. 7B and C). This effect was not observed at the same level for BPC and BPC-H_2O_2 (Fig. 7E and F). The production of smaller particles can also be confirmed by the increase in surface area (SA) after ball-milling and functionalization (Table 1) of PCSi (SA = 1 $m^2 g^{-1}$) to BPCSi-H_2O_2 (SA = 26 $m^2 g^{-1}$), while the transformation of PC to BPC-H_2O_2 did not impact the surface area (~1 $m^2 g^{-1}$). Silica is a hard material that enhances the efficiency of ball-milling[10,64,83] by promoting particle size reduction, which may also explain the improved activity of BPCSi-H_2O_2, as smaller particles are associated with reduced diffusion limitations.[84] Therefore, the promotional effect of SiO_2 in petcoke-derived solid acid catalysts was attributed to a combined effect of enhancing particle size reduction during mechanical treatment (ball milling) and formation of silanol groups that act as hydrogen-bond donors for the reactants, helping the catalysis – effects that are less pronounced in samples with a small content of SiO_2.

Although the stability of petcoke-derived solid acid catalysts was limited, valuable insights were gained regarding the functionalization of petcoke with hydrogen peroxide and nitric acid. These findings can be applied broadly to the production of carbon materials, enabling tailored control of surface oxygen-containing groups to meet specific application requirements. If a higher degree of oxidation is required on the surface, HNO_3 can be applied, while H_2O_2 will generate fewer oxygen-containing carbon groups on the surface. Moreover, the leaching of sulfonic acid sites observed for these materials is promoted by water in solution. Hence, applying these catalysts to gas-phase reactions, such as dehydration, may offer improved site stability. Additionally, the SiO_2 promoting effect emphasizes the importance of considering the impact of feedstock contamination on the valorization of waste materials. In the context of petcoke catalysts, the observed effects were advantageous for a better activity, however, this outcome may not necessarily apply to other catalytic systems.

Conclusions

Hydrogen peroxide was used to oxidize inherent sulfur species in petcoke, producing sulfonic acid sites ($-SO_3H$) that act as

active groups for esterification. Hydrogen peroxide is a more environmentally friendly functionalization agent than HNO_3. The H_2O_2-prepared catalyst (BPCSi-H_2O_2) achieved a 54% ester yield, higher than BPCSi-HNO_3 (45%), though both were less active than the commercial Amberlyst-15 catalyst (65%). Petcoke-derived catalysts were unstable and not regenerable, a common issue for carbon-based solid acid catalysts. BPCSi-H_2O_2 had fewer oxygen-containing carbon groups (~1 mmol g^{-1}) than BPCSi-HNO_3 (~5 mmol g^{-1}), which improved its activity. Despite a lower –SO_3H concentration (0.09 mmol g^{-1} *vs.* 0.14 mmol g^{-1}), BPCSi-H_2O_2 had a higher TOF than BPCSi-HNO_3 (308 *vs.* 192 h^{-1}). Increasing sulfonic acid site concentration while minimizing oxygen-containing carbon groups could enhance catalyst performance.

A higher initial SiO_2 content in petcoke helped improving the catalytic performance, as silica reduced particle size during ball milling and generated more silanol groups that helped the catalytic process. The promoting effect of SiO_2 illustrates the importance of not overlooking impurities in the feedstock when working with waste-derived materials, because they can play an important role in the overall process.

Author contributions

N. M. C.: data curation; formal analysis; investigation; methodology; validation; visualization; writing – original draft. J. M. H.: conceptualization; funding acquisition; methodology; project administration; resources; supervision; validation; visualization; writing – original draft.

Conflicts of interest

There are no conflicts to declare.

Data availability

The data supporting this article has been included as part of the supplementary information (SI). Supplementary information: Fig. S1: ester yield of petcoke-derived solid acid catalysts treated with H_2O_2 for two consecutive runs. Reaction conditions: methanol : octanoic acid molar ratio of 10 : 1, 5 wt% of catalyst, 60 °C, 800 rpm; Fig. S2: thermogravimetric analysis results: (A) TGA prolife of PCSi, BPCSi-HNO_3, and BPCSi-H_2O_2, and (B) TGA profile of PC and BPC-H_2O_2. Collected at 20 °C min^{-1} to 750 °C in a 50 mL min^{-1} flow of air; Fig. S3: ATR-FITR spectra of PCSi, ball-milled PCSi (BPCSi), and silica sand sample (SiO_2) with particle size range 300–600 μm; Fig. S4: XPS survey spectra of PC, PCSi, and chemically treated samples; Fig. S5: ATR-FTIR (A) comparing PCSi *versus* PC, and BPCSi-H_2O_2 versus BPC-H_2O_2 in the 500–2000 cm^{-1} region; (B) full range (4000–500 cm^{-1}) for all samples; Fig. S6: high-resolution XPS spectra of petcoke-derived samples before (PC and PCSi) and after treatment with hydrogen peroxide (BPCSi-H_2O_2 and BPC-H_2O_2), C 1s (left) and S 2p (right); Table S1: esterification reactions over different waste-derived carbon-based solid acid catalysts and Amberlyst-15; Table S2: elemental analysis of petcoke and petcoke-derived catalysts; Table S3: surface elemental analysis calculated from XPS survey spectrum (wt%); Table S4: Area% of deconvoluted signals from XPS high-resolution data. See DOI: https://doi.org/10.1039/d5ra05900c.

Acknowledgements

The authors would like to acknowledge funding from the Natural Sciences and Research Council (NSERC Discovery Grant #RGPIN/03882-2020).

References

1 J. M. Hill, A. Karimi and M. Malekshahian, Characterization, gasification, activation, and potential uses for the millions of tonnes of petroleum coke produced in Canada each year, *Can. J. Chem. Eng.*, 2014, **92**(9), 1618–1626.
2 United Nations Statistics Division, UNdata | record view | Petroleum Coke [Internet], 2023, [cited 2025 Jun 4]. Available from: http://data.un.org/Data.aspx?d=EDATA&f=cmID%3APK.
3 G. Xu, Atmospheric Benzo[a]pyrene and vanadium evidence for the presence of petroleum coke dust in the Athabasca Oil Sands Region, *J. Clean. Prod.*, 2018, **171**, 592–599.
4 S. G. Almalki, W. H. Alshitari and A. A. Yakout, An insight into the utilization of high-sulfur green Saudi Arabian petcoke as an ecofriendly sorbent for enhanced simultaneous sequestration of heavy metal ions from industrial wastewaters, *Pet. Sci. Technol.*, 2024, 1–20.
5 R. L. B. Cabral, E. R. V. P. Galvão, P. B. A. Fechine, F. M. F. Galvão and J. H. O. do Nascimento, A minireview on the utilization of petroleum coke as a precursor for carbon-based nanomaterials (CNMs): perspectives and potential applications, *RSC Adv.*, 2024, **14**(28), 19953–19968.
6 D. Mandal, P. L. Mahapatra, R. Kumari, P. Kumbhakar, A. Biswas, B. Lahiri, *et al.*, Convert waste petroleum coke to multi-heteroatom self-doped graphene and its application as supercapacitors, *Emergent Mater.*, 2021, **4**(2), 531–544.
7 J. A. Arcibar-Orozco, H. E. Zili-Tomita, V. A. Suárez-Toriello and J. O. Saucedo-Lucero, Petcoke Revalorization as Support for ZnO-based Photocatalyst, *Waste Biomass Valorization*, 2022, **13**(3), 1681–1694.
8 Q. He, J. Yu, X. Song, L. Ding, J. Wei and G. Yu, Utilization of biomass ash for upgrading petroleum coke gasification: Effect of soluble and insoluble components, *Energy*, 2020, **192**, 116642.
9 J. Olmeda, M. I. Sánchez de Rojas, M. Frías, S. Donatello and C. R. Cheeseman, Effect of petroleum (pet) coke addition on the density and thermal conductivity of cement pastes and mortars, *Fuel*, 2013, **107**, 138–146.
10 Y. Xiao and J. M. Hill, Solid acid catalysts produced by sulfonation of petroleum coke: Dominant role of aromatic hydrogen, *Chemosphere*, 2020, 248.
11 S. Liu, H. Wang, P. Neumann, C. S. Kim and K. J. Smith, Esterification over Acid-Treated Mesoporous Carbon Derived from Petroleum Coke, *ACS Omega*, 2019, **4**(3), 6050–6058.

12 Q. Huang, A. S. Schafranski, M. J. Hazlett, Y. Xiao and J. M. Hill, Nitric Acid Functionalization of Petroleum Coke to Access Inherent Sulfur, *Catalysts*, 2020, **10**(2), 259.
13 Q. Huang, N. M. Cabral, X. Tong, A. S. Schafranski, P. Kennepohl and J. M. Hill, Preparation of Carbon-Based Solid Acid Catalyst from High-Sulfur Petroleum Coke with Nitric Acid and Ball Milling, and a Computational Evaluation of Inherent Sulfur Conversion Pathways, *Molecules*, 2023, **28**(20), 7051.
14 P. Luo, Z. Chen, X. Chen and W. Ma, Deep Desulfurization of High-Sulfur Petroleum Coke *via* Alkali Catalytic Roasting Combined with Ultrasonic Oxidation, *Materials*, 2024, **17**(11), 2609.
15 X. Yu, D. Yu, G. Yu, F. Liu, J. Han, J. Wu, *et al.*, Temperature-resolved evolution and speciation of sulfur during pyrolysis of a high-sulfur petroleum coke, *Fuel*, 2021, **295**, 120609.
16 J. Shan, J. jie Huang, Li J. zhou, G. Li, J. tao Zhao and F. Y. tian, Insight into transformation of sulfur species during KOH activation of high sulfur petroleum coke, *Fuel*, 2018, **215**, 258–265.
17 Y. Wang, Y. Yu, R. Jia, C. Zhang and B. Zhang, Electrochemical synthesis of nitric acid from air and ammonia through waste utilization, *Natl. Sci. Rev.*, 2019, **6**(4), 730–738.
18 M. Wu, Y. Wang, D. Wang, M. Tan, P. Li, W. Wu, *et al.*, SO3H-modified petroleum coke derived porous carbon as an efficient solid acid catalyst for esterification of oleic acid, *J. Porous Mater.*, 2016, **23**(1), 263–271.
19 D. Zeng, S. Liu, W. Gong, G. Wang, J. Qiu and Y. Tian, Acid properties of solid acid from petroleum coke by chemical activation and sulfonation, *Catal. Commun.*, 2013, **40**, 5–8.
20 J. Wu, V. Montes, L. D. Virla and J. M. Hill, Impacts of amount of chemical agent and addition of steam for activation of petroleum coke with KOH or NaOH, *Fuel Process. Technol.*, 2018, **181**, 53–60.
21 B. Panchal, Y. Sun, C. Zhao, J. Wang, K. Bian, Q. Zhao, *et al.*, Waste to value addition: Utilization of waste corn cob from corn plant derived novel green acidic catalyst for effective synthesis of esters, *Energy Rep.*, 2024, **11**, 4277–4289.
22 M. F. Hussein, A. O. Abo El Naga, S. M. El, M. M. AbuBaker, S. A. Shaban and F. Y. El Kady, Potato peel waste-derived carbon-based solid acid for the esterification of oleic acid to biodiesel, *Environ. Technol. Innov.*, 2021, **21**, 101355.
23 H. Yu, Y. Cao, H. Li, G. Zhao, X. Zhang, S. Cheng, *et al.*, An efficient heterogeneous acid catalyst derived from waste ginger straw for biodiesel production, *Renew. Energy*, 2021, **176**, 533–542.
24 H. Yu, Z. Yu, Q. Shao, S. Cheng, C. Ren, G. Liu, *et al.*, Preparation of a garlic peel waste-derived carbon solid acid catalyst with the porous structure for biodiesel production, *Biomass Convers. Biorefin.*, 2024, **14**(4), 5411–5422.
25 K. Ngaosuwan, J. G. Goodwin and P. Prasertdham, A green sulfonated carbon-based catalyst derived from coffee residue for esterification, *Renew. Energy*, 2016, **86**, 262–269.
26 R. C. Agapay, H. C. Liu, Y. H. Ju, A. W. Go, A. E. Angkawijaya, P. L. T. Nguyen, *et al.*, Synthesis and Initial Evaluation of Solid Acid Catalyst Derived from Spent Coffee Grounds for the Esterification of Oleic Acid and Methanol, *Waste Biomass Valorization*, 2021, **12**(8), 4387–4397.
27 R. Berenguer, J. P. Marco-Lozar, C. Quijada, D. Cazorla-Amorós and E. Morallón, A comparison between oxidation of activated carbon by electrochemical and chemical treatments, *Carbon*, 2012, **50**(3), 1123–1134.
28 G. Singer, P. Siedlaczek, G. Sinn, H. Rennhofer, M. Mičušík, M. Omastová, *et al.*, Acid Free Oxidation and Simple Dispersion Method of MWCNT for High-Performance CFRP, *Nanomaterials*, 2018, **8**(11), 912.
29 Y. Zhang, W. Shotyk, C. Zaccone, T. Noernberg, R. Pelletier, B. Bicalho, *et al.*, Airborne Petcoke Dust is a Major Source of Polycyclic Aromatic Hydrocarbons in the Athabasca Oil Sands Region, *Environ. Sci. Technol.*, 2016, **50**(4), 1711–1720.
30 J. Caruso, K. Zhang, N. Schroeck, B. McCoy and S. McElmurry, Petroleum Coke in the Urban Environment: A Review of Potential Health Effects, *Int. Res. J. Publ. Environ. Health*, 2015, **12**(6), 6218–6231.
31 C. A. Manzano, C. Marvin, D. Muir, T. Harner, J. Martin and Y. Zhang, Heterocyclic Aromatics in Petroleum Coke, Snow, Lake Sediments, and Air Samples from the Athabasca Oil Sands Region, *Environ. Sci. Technol.*, 2017, **51**(10), 5445–5453.
32 I. L. Motta, R. A. Arnold, F. J. Lopez-Tenllado, R. M. Filho, M. R. Wolf Maciel and J. M. Hill, CO2 gasification of sugarcane bagasse char: Consideration of pyrolysis temperature, silicon and aluminum contents, and potassium addition for recirculation of char, *Energy Fuels*, 2020, **34**(12), 16201–16211.
33 D. Hernández-Martínez, A. A. Leyva-Verduzco, F. Rodríguez-Félix, M. Acosta-Elías and F. J. Wong-Corral, Obtaining and characterization of silicon(Si) from wheat husk ash for its possible application in solar cells, *J. Clean. Prod.*, 2020, **271**, 122698.
34 D. Álvarez López and M. García García, Analysis of the Impact of the Coke Manufacturing Process on the Service Life of Siliceous Refractory, *Appl. Sci.*, 2022, **12**(24), 13015.
35 J. Liu, X. Wang, H. Wang, H. Xu and J. Yang, Preparation and anti-coking application of sol–gel SiO_2 coating in a delayed coking furnace, *RSC Adv.*, 2021, **11**(17), 9849–9855.
36 C. A. Morales-Paredes, I. Rodríguez-Linzán, M. D. Saquete, R. Luque, S. M. Osman, N. Boluda-Botella, *et al.*, Silica-derived materials from agro-industrial waste biomass: Characterization and comparative studies, *Environ. Res.*, 2023, **231**, 116002.
37 L. Puri, Y. Hu and G. Naterer, Critical review of the role of ash content and composition in biomass pyrolysis, *Front. Bioenergy Biofuels*, 2024, **2**.
38 W. K. Setiawan and K. Y. Chiang, Crop Residues as Potential Sustainable Precursors for Developing Silica Materials: A Review, *Waste Biomass Valorization*, 2021, **12**(5), 2207–2236.
39 M. A. Taiye, W. Hafida, F. Kong and C. Zhou, A review of the use of rice husk silica as a sustainable alternative to traditional silica sources in various applications, *Environ. Prog. Sustain. Energy*, 2024, **43**(6).

40 A. J. Bowles and G. D. Fowler, Assessing the impacts of feedstock and process control on pyrolysis outputs for tyre recycling, *Resour. Conserv. Recycl.*, 2022, **182**, 106277.
41 X. Dai, Y. Xu and B. Dong, Effect of the micron-sized silica particles (MSSP) on biogas conversion of sewage sludge, *Water Res.*, 2017, **115**, 220–228.
42 J. W. Pinder, G. H. Major, D. R. Baer, J. Terry, J. E. Whitten, J. Čechal, *et al.*, Avoiding common errors in X-ray photoelectron spectroscopy data collection and analysis, and properly reporting instrument parameters, *Appl. Surf. Sci. Adv.*, 2024, **19**, 100534.
43 Y. M. Maldonado, I. L. Alonso-Lemus, C. R. Sarabia-Castillo, B. Escobar-Morales, L. J. Ríos-González, F. Fernández-Luqueño, *et al.*, Sewage sludge-derived biocarbons as catalysts of bioanodes in a dual-chamber microbial fuel cell using nejayote as substrate, *Int. J. Hydrogen Energy*, 2025, **108**, 185–197.
44 X. Yang, H. Guo, X. Cao, Y. Ma, W. Wang and N. Guo, Solid Acid Catalyst Derived from Cotton for Conversion of Xylose and Corn Cob to Furfural, *ChemistrySelect*, 2022, **7**(46).
45 T. Fan, R. Zhang, J. Feng and H. Pan, Directional Catalytic Conversion of Biomass Carbohydrates into High Added-value Levulinates with Bifunctionalized Metal-supported Carbon-based Catalyst, *ChemistrySelect*, 2023, **8**(26).
46 W. Li and T. J. Bandosz, Analyzing the effect of nitrogen/sulfur groups' density ratio in porous carbons on the efficiency of CO2 electrochemical reduction, *Appl. Surf. Sci.*, 2021, **569**, 151066.
47 M. Sevilla and A. B. Fuertes, Highly porous S-doped carbons, *Microporous Mesoporous Mater.*, 2012, **158**, 318–323.
48 J. Feng, G. Wen, W. Huang, E. T. Kang and K. G. Neoh, Influence of oxygen plasma treatment on poly(ether sulphone) films, *Polym. Degrad. Stab.*, 2006, **91**(1), 12–20.
49 C. A. D. S. Moura, G. K. Belmonte, P. G. Reddy, K. E. Gonslaves and D. E. Weibel, EUV photofragmentation study of hybrid nonchemically amplified resists containing antimony as an absorption enhancer, *RSC Adv.*, 2018, **8**(20), 10930–10938.
50 Y. Zhang, Q. Yu, H. Wang and M. Zou, Study on the performance of petroleum coke after electrolytic desulfurization in NaBr-CH $_3$ COOH system, *Energy Sources, Part A Recovery, Util. Environ. Eff.*, 2021, 1–16.
51 P. Patel, R. K. Tak, B. Parmar, S. Dabas, B. Patel, E. Suresh, *et al.*, Ring-opening hydrolysis of spiro-epoxyoxindoles using a reusable sulfonic acid functionalized nitrogen rich carbon catalyst, *RSC Adv.*, 2021, **11**(21), 12808–12814.
52 Q. Zhang, X. Liu, T. Yang, C. Yue, Q. Pu and Y. Zhang, Facile synthesis of polyoxometalates tethered to post Fe-BTC frameworks for esterification of free fatty acids to biodiesel, *RSC Adv.*, 2019, **9**(14), 8113–8120.
53 S. Kamal, Catalyst deactivation of cation-exchange resin in c <scp>ross-aldol</scp> condensation of acetaldehyde to methyl pentenone, *Flavour Fragrance J.*, 2023, **38**(4), 312–325.
54 Y. LIU, E. LOTERO and J. GOODWINJR, Effect of carbon chain length on esterification of carboxylic acids with methanol using acid catalysis, *J. Catal.*, 2006, **243**(2), 221–228.
55 J. M. Fraile, E. García-Bordejé, E. Pires and L. Roldán, Catalytic performance and deactivation of sulfonated hydrothermal carbon in the esterification of fatty acids: Comparison with sulfonic solids of different nature, *J. Catal.*, 2015, **324**, 107–118.
56 R. A. Elshwehy, M. M. Fawzy, F. Fakhry and M. M. Hamdy, High-purity kaolinite-based electrodes for supercapacitor application: New approach of the Egyptian silica sand added-value, *J. Alloys Compd. Commun.*, 2025, **8**, 100110.
57 S. Dwivedi, M. Yadav, A. K. Singh, A. K. Sharma, M. K. Jaiswal, M. M. Dwivedi, *et al.*, Assessment of toxicity in silica sand tailings—a case study of Shankargarh area of Prayagraj, India, *Environ. Monit. Assess.*, 2025, **197**(10), 1116.
58 M. Osacky, M. Geramian, D. G. Ivey, Q. Liu and T. H. Etsell, Mineralogical and chemical composition of petrologic end members of Alberta oil sands, *Fuel*, 2013, **113**, 148–157.
59 X. Cui, Y. Wang, L. Wang, L. Cui and M. Qi, SYNTHESIS OF NANOMETER-SIZED TiC AND SiC FROM PETROLEUM COKE BY REACTIVE MILLING, *Pet. Sci. Technol.*, 2001, **19**(7–8), 971–978.
60 K. A. Fitria, M. Dewa, J. Liu, S. Ha and B. Yang, Development of sulfonated carbon-based solid-acid catalysts derived from biorefinery residues and biomass ash for xylan hydrolysis, *Bioresour. Technol. Rep.*, 2023, **24**, 101607.
61 A. P. da Luz Corrêa, R. R. C. Bastos, G. N. da Rocha Filho, J. R. Zamian and L. R. V. da Conceição, Preparation of sulfonated carbon-based catalysts from murumuru kernel shell and their performance in the esterification reaction, *RSC Adv.*, 2020, **10**(34), 20245–20256.
62 A. Hani, N. Meftah, L. Zeghoud, A. Sdiri and A. H. Jawad, Statistical Optimization and Desirability Function for Producing Nano Silica from Dune Sand by Sol–gel Method Towards Methylene Blue Dye Removal, *J. Inorg. Organomet. Polym. Mater.*, 2023, **33**(7), 1882–1897.
63 R. Ellerbrock, M. Stein and J. Schaller, Comparing amorphous silica, short-range-ordered silicates and silicic acid species by FTIR, *Sci. Res.*, 2022, **12**(1), 11708.
64 F. J. Lopez-Tenllado, I. L. Motta and J. M. Hill, Modification of biochar with high-energy ball milling: Development of porosity and surface acid functional groups, *Bioresour. Technol. Rep.*, 2021, **15**, 100704.
65 M. Ahmadian and M. Anbia, Highly efficient oxidative desulfurization catalyzed by copper-based materials using hydrogen peroxide as oxidant, *Fuel*, 2022, **15**, 324.
66 N. d'Alessandro, L. Tonucci, M. Bonetti, M. Di Deo, M. Bressan and A. Morvillo, Oxidation of dibenzothiophene by hydrogen peroxide or monopersulfate and metal–sulfophthalocyanine catalysts: an easy access to biphenylsultone or 2-(2′-hydroxybiphenyl) sulfonate under mild conditions, *New J. Chem.*, 2003, **27**(6), 989–993.
67 J. Shao, Y. Wang, M. Che, Y. Liu, Y. Jiang, Q. Xiao, *et al.*, Sustainable CO2 Capture: N,S-Codoped Porous Carbons Derived from Petroleum Coke with High Selectivity and Stability, *Molecules [Internet]*, 2025, **30**(2), 426.
68 J. J. Ternero-Hidalgo, J. M. Rosas, J. Palomo, M. J. Valero-Romero, J. Rodríguez-Mirasol and T. Cordero,

Functionalization of activated carbons by HNO3 treatment: Influence of phosphorus surface groups, *Carbon*, 2016, **101**, 409–419.

69 L. Dalstein, E. Potapova and E. Tyrode, The elusive silica/water interface: isolated silanols under water as revealed by vibrational sum frequency spectroscopy, *Phys. Chem. Chem. Phys.*, 2017, **19**(16), 10343–10349.

70 C. Van Hoang, D. N. Thoai, N. T. D. Cam, T. T. T. Phuong, N. T. Lieu, T. T. T. Hien, *et al.*, Large-Scale Synthesis of Nanosilica from Silica Sand for Plant Stimulant Applications, *ACS Omega*, 2022, 7(45), 41687–41695.

71 J. Schönherr, J. Buchheim, P. Scholz and P. Adelhelm, Boehm Titration Revisited (Part I): Practical Aspects for Achieving a High Precision in Quantifying Oxygen-Containing Surface Groups on Carbon Materials, *C (Basel)*, 2018, **4**(2), 21.

72 K. Sun, J. Jin, M. Keiluweit, M. Kleber, Z. Wang, Z. Pan, *et al.*, Polar and aliphatic domains regulate sorption of phthalic acid esters (PAEs) to biochars, *Bioresour. Technol.*, 2012, **118**, 120–127.

73 E. T. Özer and Ş. Güçer, Determination of some phthalate acid esters in artificial saliva by gas chromatography–mass spectrometry after activated carbon enrichment, *Talanta*, 2011, **84**(2), 362–367.

74 B. Zhang, M. Gao, J. Geng, Y. Cheng, X. Wang, C. Wu, *et al.*, Catalytic performance and deactivation mechanism of a one-step sulfonated carbon-based solid-acid catalyst in an esterification reaction, *Renew. Energy*, 2021, **164**, 824–832.

75 L. J. Konwar, P. Mäki-Arvela and J. P. Mikkola, SO_3 H-Containing Functional Carbon Materials: Synthesis, Structure, and Acid Catalysis, *Chem. Rev.*, 2019, **119**(22), 11576–11630.

76 J. Li, Y. J. Fu, X. J. Qu, W. Wang, M. Luo, C. J. Zhao, *et al.*, Biodiesel production from yellow horn (Xanthoceras sorbifolia Bunge.) seed oil using ion exchange resin as heterogeneous catalyst, *Bioresour. Technol.*, 2012, **108**, 112–118.

77 R. Tesser, L. Casale, D. Verde, M. Di Serio and E. Santacesaria, Kinetics and modeling of fatty acids esterification on acid exchange resins, *Chem. Eng. J.*, 2010, **157**(2–3), 539–550.

78 J. M. Fraile, E. García-Bordejé, E. Pires and L. Roldán, New insights into the strength and accessibility of acid sites of sulfonated hydrothermal carbon, *Carbon*, 2014, **77**, 1157–1167.

79 I. J. McLaws, Silica sands in the Fort McMurray area, Alberta; Alberta Research Council, *ARC/AGS Economic Geology Report*, 1980, **6**, 61.

80 A. M. Chibiryaev, I. V. Kozhevnikov and O. N. Martyanov, High-temperature reaction of SiO2 with methanol: Nucleophilic assistance of some N-unsubstituted benzazoles, *Appl. Catal., A*, 2013, **456**, 159–167.

81 A. A. Tsyganenko, E. N. Storozheva, O. V. Manoilova, T. Lesage, M. Daturi and J. C. Lavalley, Brønsted acidity of silica silanol groups induced by adsorption of acids, *Catal. Lett.*, 2000, **70**(3–4), 159–163.

82 M. Sulpizi, M. P. Gaigeot and M. Sprik, The Silica–Water Interface: How the Silanols Determine the Surface Acidity and Modulate the Water Properties, *J. Chem. Theor. Comput.*, 2012, **8**(3), 1037–1047.

83 Y. Yu, J. Huang, W. Zhang, K. Zhang, S. Deng and G. Yu, Mechanochemical destruction of mirex co-ground with iron and quartz in a planetary ball mill, *Chemosphere*, 2013, **90**(5), 1729–1735.

84 R. Klaewkla, M. Arend and F. W, A Review of Mass Transfer Controlling the Reaction Rate in Heterogeneous Catalytic Systems. In: *Mass Transfer - Advanced Aspects [Internet]*, InTech, 2011, **http://www.intechopen.com/books/mass-transfer-advanced-aspects/a-review-of-mass-transfer-controlling-the-reaction-rate-in-heterogeneous-catalytic-systems**.